Reg Environ Change
DOI 10.1007/s10113-013-0477-8

ORIGINAL ARTICLE

On the twenty-first-century wet season projections over the Southeastern United States

Christopher Selman · Vasu Misra · Lydia Stefanova · Steven Dinapoli · Thomas J. Smith III

Received: 10 July 2012 / Accepted: 8 May 2013

Abstract This paper reconciles the difference in the projections of the wet season over the Southeastern United States (SEUS) from a global climate model (the Community Climate System Model Version 3 [CCSM3]) and from a regional climate model (the Regional Spectral Model [RSM]) nested in the CCSM3. The CCSM3 projects a dipole in the summer precipitation anomaly: peninsular Florida dries in the future climate, and the remainder of the SEUS region becomes wetter. The RSM forced with CCSM3 projects a universal drying of the SEUS in the late twenty-first century relative to the corresponding twentieth-century summer. The CCSM3 pattern is attributed to the "upped-ante" mechanism, whereby the atmospheric boundary layer moisture required for convection increases in a warm, statically stable global tropical environment. This criterion becomes harder to meet along convective margins, which include peninsular Florida, resulting in its drying. CCSM3 also projects a southwestward expansion of the North Atlantic subtropical high that leads to further stabilizing of the atmosphere above Florida, inhibiting convection. The RSM, because of its high (10-km grid) resolution, simulates diurnal variations in summer rainfall over SEUS reasonably well. The RSM improves upon CCSM3 through the RSM's depiction of the diurnal variance of precipitation, which according to observations accounts for up to 40 % of total seasonal precipitation variance. In the future climate, the RSM projects a significant reduction in the diurnal variability of convection. The reduction is attributed to large-scale stabilization of the atmosphere in the CCSM3 projections.

Keywords Regional climate change · Southeast United States · Rainfall variability · Regional climate model · Global climate model · Precipitation variability

C. Selman (✉) · V. Misra
Department of Earth, Ocean and Atmospheric Science, Florida State University, Tallahassee, FL, USA
e-mail: cms05j@my.fsu.edu

C. Selman · V. Misra · L. Stefanova · S. Dinapoli
Center for Ocean-Atmospheric Prediction Studies, Florida State University, Tallahassee, FL, USA

V. Misra
Florida Climate Institute, Florida State University, Tallahassee, FL, USA

T. J. Smith III
Southeastern Ecological Science Center, United States Geological Survey, St. Petersburg, FL, USA

Introduction

There is a growing demand among policymakers for regionally downscaled climate projections. Current global projections are on the order of hundreds of kilometers, which is too coarse to use for decision-making. Furthermore, low-resolution models may not be adequate for resolving local surface features. Failing to resolve significant features such as coastlines or orography may severely hinder global climate projections. As a response to the growing demand, many downscaled modeling products have been developed, such as the European ENSEMBLES project (Doblas-Reyes and Goodess 2005) or the North American Regional Climate Change Assessment Program (NARCCAP) (Mearns et al. 2009).

NARCCAP presents users with easily accessible, dynamically downscaled data of global climate model projections over North America. NARCCAP model

Published online: 22 May 2013

integrations cover periods of 1971–2000 and 2041–2070 that are representative of the current and future climate. Mean twenty-first century summer rainfall projections vary depending on the pairing of GCM and RCM. For instance, one of the NARCCAP regional climate models (MM5I) projects a drying of the Southeast United States (SEUS) when forced with the global CCSM3 data. When the same regional model is forced with global HadCM3 data, the MM5I projects an increase in summer precipitation over the SEUS. NARCCAP offers eleven such pairings of global and regional models. Sobolowski and Pavelski (2011) used a reliability ensemble averaging technique to weight and determine model projections of precipitation in NARCCAP models. Weighted rainfall averages were seen to be heterogeneous in sign and magnitude across the domain. Only the area west of the Mississippi River was seen to be consistently drier in a future climate. Elguindi and Grundstein (2013) noted, however, that much of the SEUS would have a lower moisture index under the Thornthwaite climate classification system in a future climate.

Of particular relevance is the diurnal variability of rainfall, which accounts for a large fraction of the total seasonal summer rainfall variability (Carbone and Tuttle 2008; Bastola and Misra 2013). Local sea breeze effects along the long SEUS coastlines are a significant contributing factor to diurnal rainfall variability (Schwartz and Bosart 1979; Biggs and Graves 1962; Atkins et al. 1995; LeMone 1973). Sea breeze variability in the SEUS peaks in the summer (Zhang et al. 2009). Orographic effects in the central SEUS also play a major role in the diurnal variability of the rainfall (Parker and Ahijevych 2007) despite the absence of persistent low-level jets (Zhang et al. 2006). The observed, infrequent low-level jets are most pronounced near the Appalachian and Blue Ridge Mountains in summer. Short-lived, convective episodes off the Appalachians accounted for 77.9 % of the summer seasonal variance in the mountainous regions (Parker and Ahijevych 2007). El Niño Southern Oscillation (ENSO) can also contribute to the variability of rainfall in the SEUS (Kushnir et al. 2010) primarily through its noted influence on landfalling tropical cyclones (Bove et al. 1998). The influence of ENSO on summer rainfall variability, however, is decadally varying and spatially sporadic over Florida and its bordering states (Misra and Dinapoli 2012). However, the modification of the diurnal variability of rainfall from global climate change could be another potential source of significant rainfall change in the SEUS.

Rainfall variability in the southern part of the SEUS is driven in part by warming of SST (Rauscher et al. 2011) in remote tropical oceans (Xie et al. 2010). Warming of equatorial Pacific SST is expected as a consequence of increases in greenhouse gas (GHG) concentrations (Vecchi et al. 2008). This anomalously warm tropical SST will likely result in reduction in SEUS rainfall (Rauscher et al. 2011), a characteristic of the "upped-ante" (also known as the "rich-get-richer") mechanism (Neelin et al. 2003). In a troposphere warmed by El Niño (Yualeva et al. 1994) or trapping of longwave radiation by increased GHG concentrations, more moist static energy (MSE) is required to initiate convection (Chiang and Sobel 2002). The source of this MSE is primarily atmospheric boundary layer (ABL) moisture. The regions abundant in ABL moisture (e.g., intertropical convergence zones) will generally convect more vigorously under a warm troposphere. But, Neelin et al. (2003) indicated that regions on the margins of these convective zones (typical subtropical regions with prevailing large-scale subsidence) would convect less in such warm environments, as the boundary layer air in these regions usually originates from relatively drier areas.

The North Atlantic Subtropical High (NASH) has been identified as another source of rainfall variability in the SEUS (Li et al. 2011; Christensen et al. 2007). Li et al. (2011) indicated that because of global warming, the NASH has become stronger and shifted westward, with a concomitant increase in the interannual variability of summer rainfall over the SEUS in the last three decades. They suggest that with the systematic westward shift of the Bermuda high in the last three decades, its meridional movement has had an increased influence on the SEUS summer season rainfall leading to its increased interannual variability.

Description of models

One global climate model and one regional climate model (nested into the global model) are used to analyze precipitation projections for the twenty-first century. The global climate model, the Community Climate System Model version 3 (CCSM3; Collins et al. 2006), is a coupled climate model whose components are summarized in Table 1. The CCSM3 integrations used in this study have 26 vertical hybrid levels, and the model uses spectral truncation of T85, which offers a horizontal resolution of approximately 1.4° by 1.4°. The CCSM3 climate integration data at six-

Table 1 Component models of the CCSM3

Component	Model
Atmosphere	Community Atmosphere Model version 3 (Collins et al. 2004, 2006)
Ocean	Parallel Ocean Program version 1.4.3 (Smith and Gent 2002)
Sea Ice	Community Sea Ice Model version 5 (Briegleb et al. 2004)
Land	Community Land Surface Model version 3 (Oleson et al. 2004; Dickinson et al. 2006)

hour intervals are obtained from the Earth System Grid (http://www.earthsystemgrid.org/).

For downscaling the CCSM3 simulation and projection, we use the Regional Spectral Model (RSM) initially developed by Juang and Kanamitsu (1994) and further developed by Kanamitsu et al. (2010). The RSM at 10-km grid resolution offers a better alternative for resolving the local orographic features of the SEUS, which are poorly represented in the native resolution of the CCSM3 (Fig. 1). For example, South Florida is under water in CCSM3, and the coastlines are ill defined. Furthermore, the height gradients of the lower Appalachians in the CCSM3 are relatively weak. The 10-km grid of the RSM rectifies some of these deficiencies. In addition, the discretization of vegetation (Fig. 2) is also relatively well resolved in the RSM. The brief outline of the RSM is provided in Table 2. Further details on RSM can be found in Kanamitsu et al. (2010) and Misra et al. (2011a).

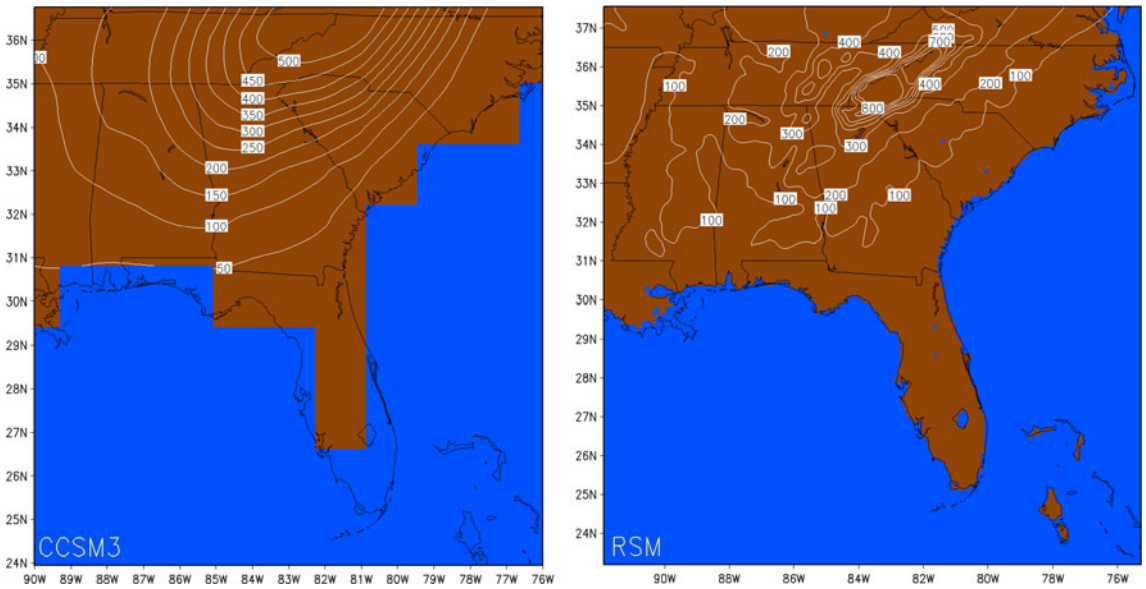

Fig. 1 Topography (contoured and in meters) and land/sea mask for CCSM3 (*left*) and RSM (*right*). *Brown* denotes land and *blue* denotes ocean points in the native resolutions of the two models

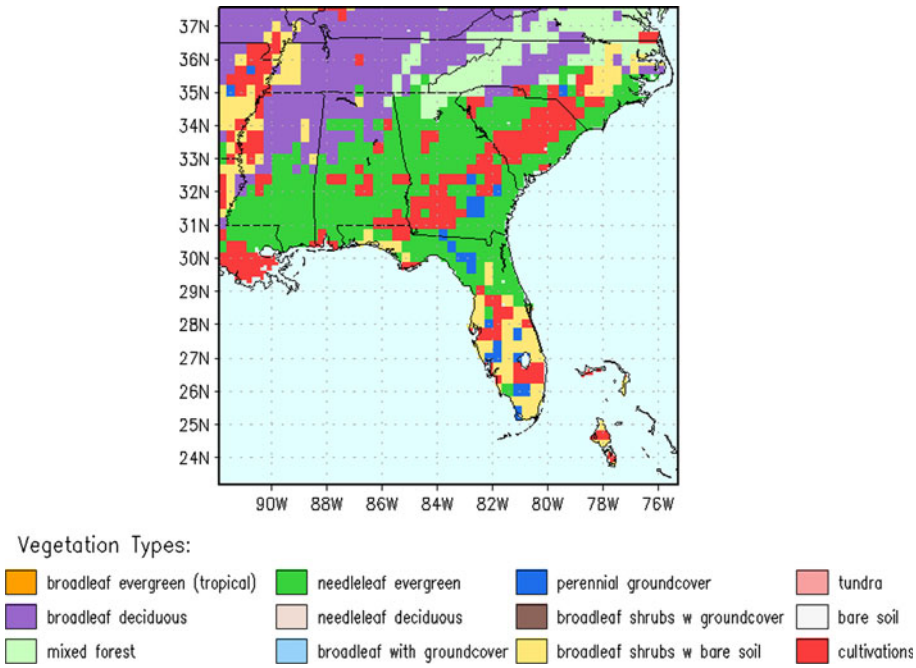

Fig. 2 Vegetation map used by RSM, adapted from the USGS vegetation map, reduced to 12 Noah vegetation types

Table 2 Surface features and parameterizations of the RSM

Feature	Description
Topography	United States Geological Survey (USGS) GTOPO30 Topography
Vegetation	USGS Vegetation reduced to 12 NOAH types (Loveland et al. 1995)
Land Surface Scheme	NOAH with four soil levels (Ek et al. 2003)
Atmospheric boundary layer Scheme	Nonlocal (Hong and Pan 1996)
Convection Scheme	Arakawa Schubert (Pan and Wu 1995)
Shortwave Scheme	Chou and Lee (1996)
Longwave Scheme	Chou and Suarez (1994)
Cloud Scheme	Relative Humidity based (Slingo 1987)

Model experiments

The RSM is forced to generate the downscaled climate for the twentieth century (hereafter, RSM20th) with output from the CCSM3 historical simulation for the years 1969–1999 (hereafter, CCSM3-20th). The downscaled region is shown in Fig. 1. The time interval of the lateral boundary forcing from the CCSM3 integration is six hours. Similarly, the RSM is forced to generate the downscaled twenty-first-century climate (hereafter, RSM21st) with output from the CCSM3 SRESA2 run (hereafter, CCSM3-21st) for the years 2040–2070.

Kanamaru and Kanamitsu (2007a) showed that the scale-selective bias correction and interior nudging of small wave numbers used by the RSM make the regional solution insensitive to the size of the regional domain and the location of lateral boundaries. This allows the nesting ratio to be much greater than that typically used in other regional models and eliminates the need for intermediate nesting. Because of this, we are able to downscale CCSM3 simulations and reanalysis data with grid resolutions on the order of 200 km directly to 10 km (Kanamaru and Kanamitsu 2007b; Kanamitsu and Kanamaru 2007; Stefanova et al. 2012). The results compare well with station and gridded observations, as well as with other high-resolution regional reanalyses. Furthermore, Misra et al. (2011a) and Stefanova et al. (2012) showed that the RSM was well suited for depicting the phase and amplitude of diurnal rainfall in the SEUS when compared with observations.

We also use the National Centers for Environmental Prediction (NCEP) Stage IV observed rainfall data available at 4-km grid resolution for the period 2002–2010 (Lin and Mitchell 2005) at hourly intervals for validation. This is a merged analysis of rain gauge and radar-based rainfall estimates available for the continental United States. This data set is used to validate the diurnal variations in the summer season rainfall in RSM20th.

Model results

Diurnal variation

As shown in earlier studies, diurnal variations in the summer climate in the SEUS are significant (Carbone and Tuttle 2008; Misra et al. 2011a, b; Stefanova et al. 2012), yet notoriously difficult for coupled global climate models to resolve (Dai 2006). In Fig. 3 we show the fraction of diurnal variations that explain the seasonal variations in summer rainfall from observations (NCEP Stage IV) and RSM20th. This fraction (F) is computed as the ratio of

$$F = \frac{\sum_{i=1}^{N} (A_i - \bar{A})^2}{\sum_{i=1}^{N} (P_i - \bar{P})^2},$$

where A is the seasonal mean diurnal amplitude, P is the seasonal mean of the total rainfall, overbars indicate

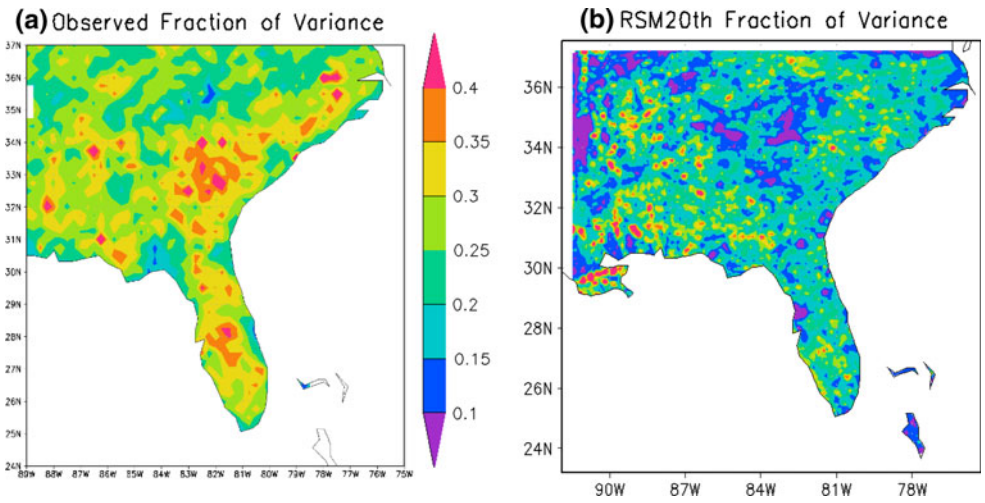

Fig. 3 **a** The diurnal fraction of variance of rainfall calculated from NCEP STAGE IV rainfall observations. **b** Similar to **a**, but calculated from RSM20th. Dimensions plotted here are fractional

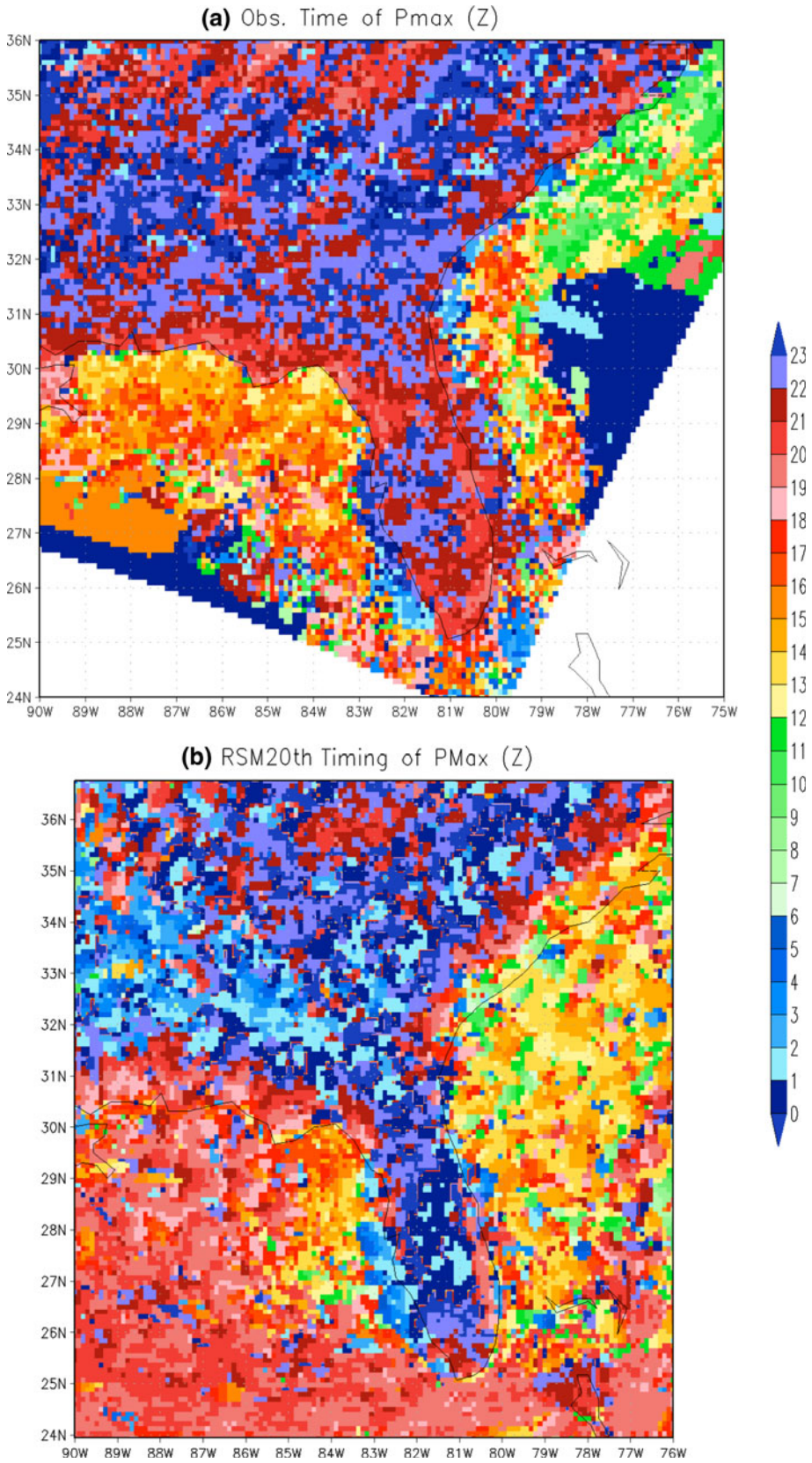

Fig. 4 **a** The observed timing of summer maximum rainfalls from NCEP STAGE IV rainfall data. **b** Timing of maximum rainfall from RSM20th. Both panels are in GMT

climatological mean, and N is the number of years (8 years for NCEP Stage IV observations and 30 years for RSM20th). RSM20th (Fig. 3b) clearly underestimates the observed fractional variance of diurnal variability (Fig. 3a). However, the observed fraction (F) is computed over an 8-year period, compared to the 30-year period of RSM20th, which could explain some of the differences in Fig. 3. It is quite apparent that in the observations the variability of diurnal rainfall explains a large fraction of the summer seasonal rainfall variability. The observed fraction ranges from 15 to 40 % in the SEUS (Fig. 3a), while in the RSM20th it ranges between 15 and 25 % (Fig. 3b), especially in the eastern half of the domain. We were unable to compute the same fraction (F) from CCSM3-20th because the data are not available at intervals shorter than 6 h.

Similarly, we have compared the diurnal phase of rainfall between NCEP Stage IV and RSM20th (Fig. 4). This figure shows the climatological hour of maximum rainfall in the summer season for observations (Fig. 4a) and for RSM20th (Fig. 4b). RSM20th can simulate this feature reasonably well over most of the SEUS, peaking between 24 and 02 GMT (~18–20 LST). However, there are some apparent disparities over the Florida panhandle and along the Carolina coasts, where the RSM20th summer rainfall tends to peak later than observations by a couple of hours.

Dai (2006), analyzing CCSM2 (which he claimed was similar in its diurnal behavior to CCSM3), showed that the timing of maximum rainfall in the summer season over SEUS was around 12–14 LST, which is roughly four to six hours earlier than observed. Similarly, Bukovsky and Karoly (2008) showed that in CCSM3 the diurnal peak of rainfall over the SEUS in the twentieth-century simulation of CCSM3 is ~1300LST (or 1900UTC). The RSM has consistently been shown to have significantly high fidelity in simulating the diurnal variability of the rainfall over the

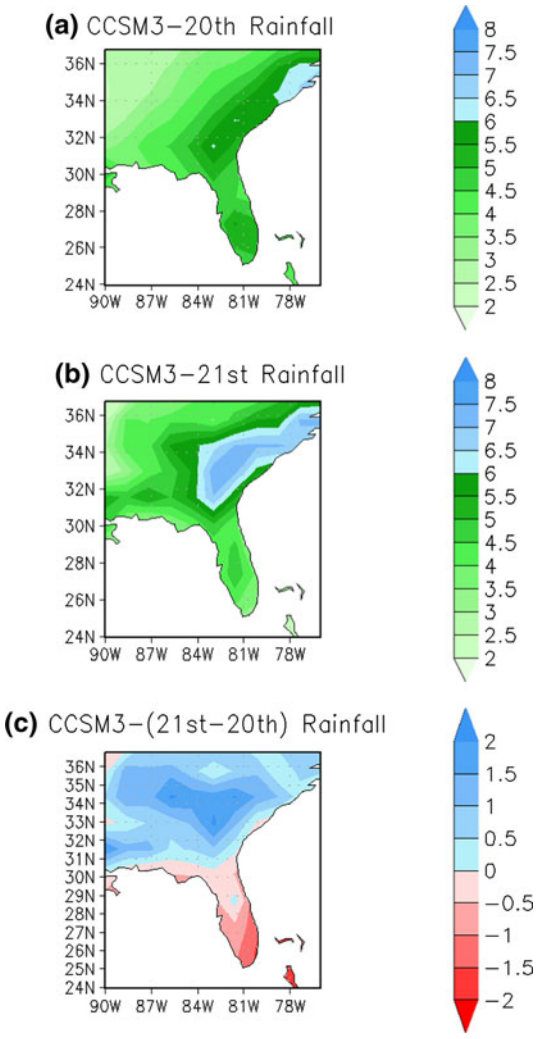

Fig. 5 June, July, and August 31-year mean rainfall from the CCSM3. Units are in mm/day. **a** The period 1969–1999. **b** The period 2040–2070. The *bottom* **c** is the difference in the two periods

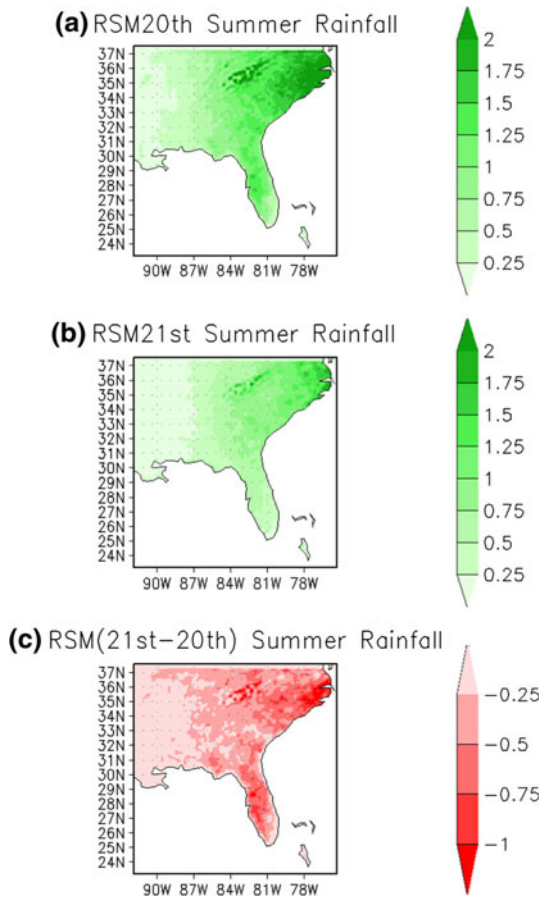

Fig. 6 June, July, and August 31-year mean rainfall from the RSM. Units are in mm/day. **a** The period 1969–1999. **b** The period 2040–2070. The bottom **c** is the difference in the two periods

SEUS (Misra et al. 2011a, b; Stefanova et al. 2012). We believe the improvement of the diurnal variations in RSM20th is largely a result of the behavior of the parameterization (especially convection) scheme in RSM at the given resolution of 10 km. Additional improvements are enhanced resolution of the orography, vegetation, and the coastlines.

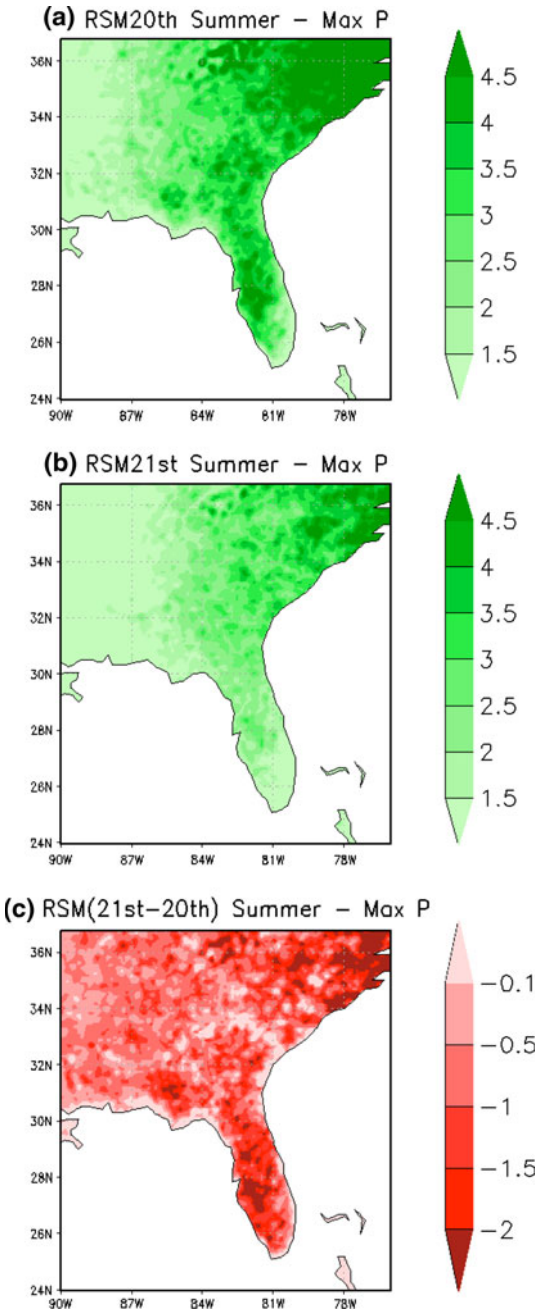

Fig. 7 **a** and **b** are RSM20th and RSM21st summer seasonal maximum rainfall, respectively. **c** A difference in the two. Units are in mm/day

Projected summer seasonal climate

Figure 5a and b shows the seasonal rainfall from CCSM3-20th and CCSM3-21st, respectively; Fig. 5c shows their differences. It is apparent from Fig. 5c that CCSM3 projects a dipole-like pattern in the twenty-first-century summer season rainfall anomaly relative to the corresponding twentieth-century seasonal rainfall: Peninsular Florida becomes drier, and the rest of the SEUS becomes wetter. This dipole pattern has also been observed by Rauscher et al. (2011), who attributed this pattern of change in the summer rainfall to the atmospheric response from remote impacts of warming in the tropical western Pacific Ocean. Figure 6a and b shows similar plots for the summer rainfall from RSM20th and RSM21st, respectively; Fig. 6c shows their difference. The pattern of rainfall anomaly (Fig. 6c) projected by RSM21st is different from that of the CCSM3, showing a universal drying of the SEUS in the late twenty-first century

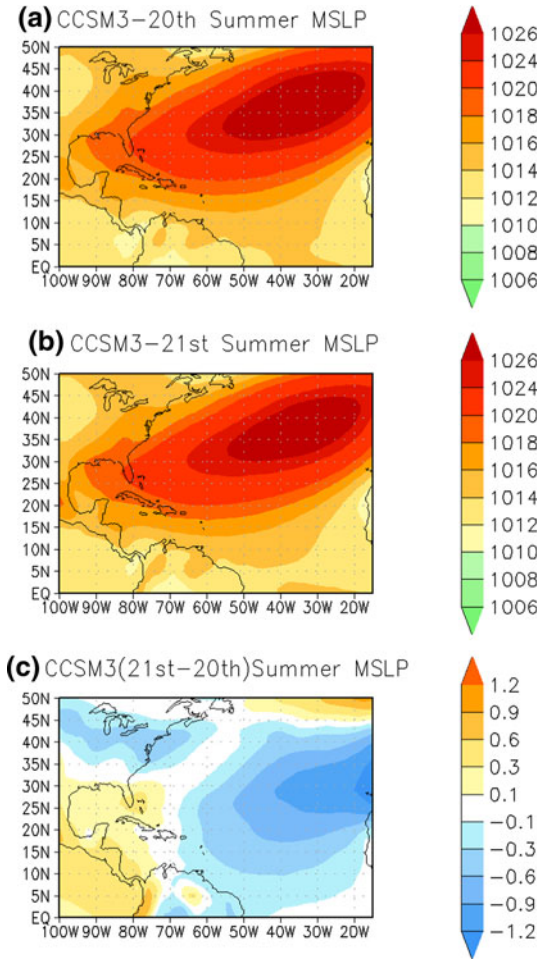

Fig. 8 **a** The CCSM3-20th mean summer sea-level pressure. **b** Similar to **a** but for CCSM3-21st. **c** The difference in the two. Units are in hPa

relative to the corresponding summer season climatology in the twentieth century. The reason for this universal drying of the summer rainfall in RSM21st is explained further in the following subsection.

Projected diurnal variations in the summer climate

Given the significance of diurnal variability to the seasonal mean summer rainfall over the SEUS, we examine RSM20th and RSM21st mean diurnal rainfall (Fig. 7). The average simulated diurnal maximum rainfall values, plotted in Fig. 7, are calculated for the climatological time of maximum precipitation. Average diurnal maximum rainfall across the SEUS in RSM20th ranges from under 1.5 mm/day to above 4.5 mm/day, with the heaviest rainfalls occurring over the eastern portion of the domain (Fig. 7). Figure 7b shows that RSM21st preserves the spatial pattern of rainfall of RSM20th, but reduces the magnitude. It becomes obvious that the diurnal rainfall at zenith has decreased across much of the SEUS in the late twenty-first century under the A2 scenario (Fig. 7c). As a result of this diminishment of diurnal rainfall at zenith, the corresponding diurnal range of rainfall is also significantly reduced in the late twenty-first century (not shown). Given that diurnal rainfall variability explains a significant fraction of the boreal summer seasonal rainfall variability (Fig. 3), we suggest that the relative drying of the total seasonal mean summer rainfall projected in RSM21st is largely a result of this reduction in the diurnal rainfall.

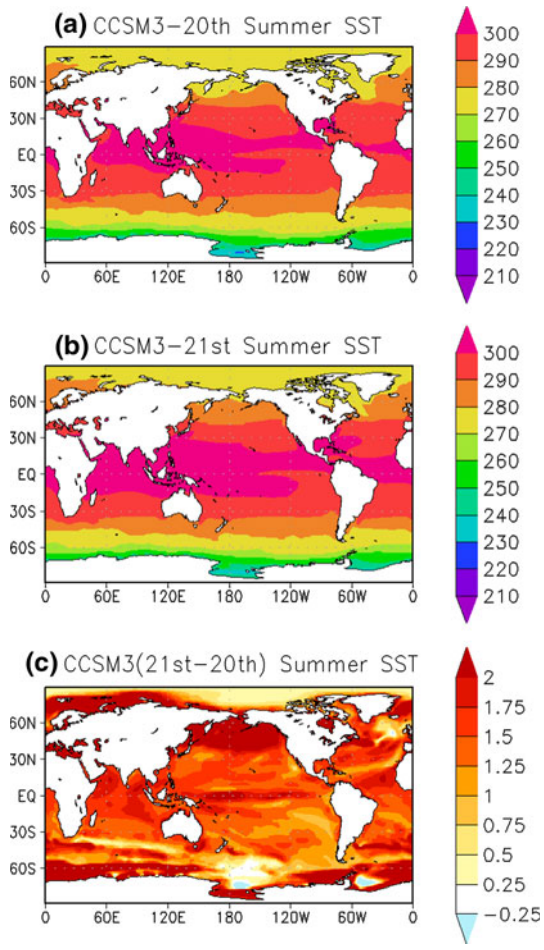

Fig. 9 **a** CCSM3-20th summer mean sea surface temperature. **b** Similar to **a**, but for CCSM3-21st. **c** The difference in the two. Units are in Kelvins

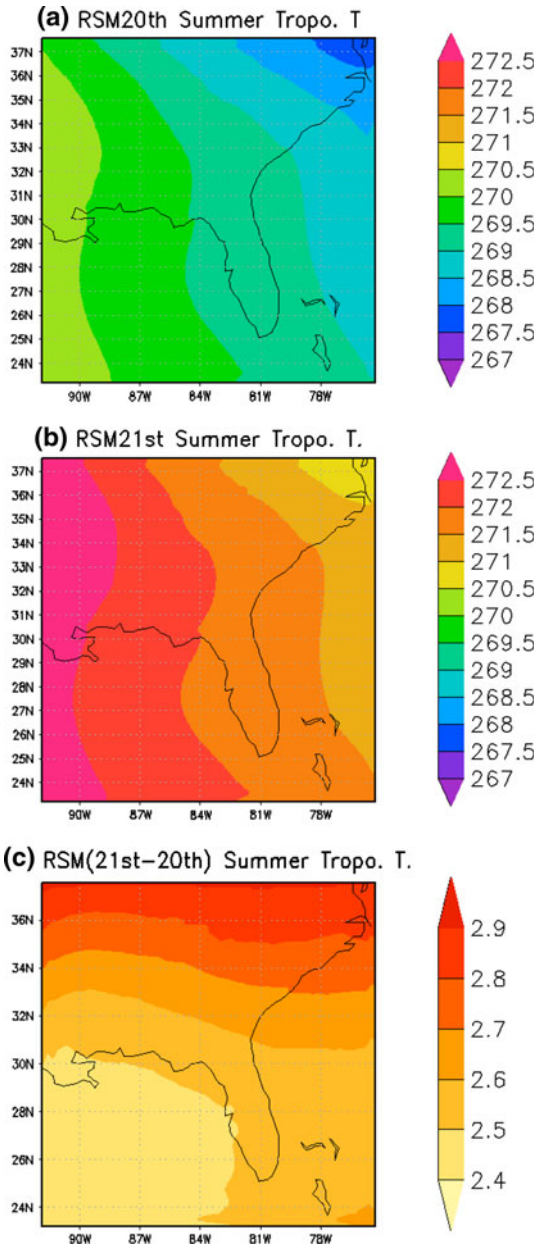

Fig. 10 **a** The RSM20th summer mean tropospheric temperature; units are in Kelvins. **b** The same as **a**, but for RSM21st. **c** The difference in the two

Discussion

What physical reasons might lead to the SEUS drying in the RSM21st simulation? Why does the RSM21st differ from CCSM3-21st? We suggest that answers to these questions will help us to reconcile the uncertainty associated with regional climate projection. In response to the first question, we propose two complementary large-scale forcing mechanisms that affect the diurnal peak rainfall: (1) the atmospheric stabilization of the SEUS environment by the westward expansion of the NASH and (2) the large-scale tropical–subtropical stabilization as a response to warming of the remote tropical Pacific Ocean. Figure 8a, b, and c shows the climatological summer seasonal mean sea-level pressure from the CCSM3-20th and the CCSM3-21st and their difference, respectively. CCSM3 projects a westward shift of the NASH, as apparent from the positive values of the differences in the sea-level pressure (Fig. 8c) over a large fraction of the SEUS domain of RSM. This westward shift of the NASH in the future projection entails large-scale subsidence in the lower troposphere that is not conducive to convection. Note that Fig. 8 is plotted from the CCSM3 integrations as the domain shown is outside the regional domain of RSM used in this study.

We see in Fig. 9a, b, and c that the climatological summer seasonal mean SST from CCSM3-20th and CCSM3-21st and their differences, respectively, support the second large-scale mechanism that we hypothesize is causing the relative drying in the RSM21st simulation. The CCSM3 projects a uniform warming of the SST over most of the global oceans in the late twenty-first century for the A2 emission scenario. Of particular note is the significant warming in the equatorial Pacific, reminiscent of anomalies associated with El Niño. We expect a uniform warming of the troposphere in the tropical–subtropical latitudes as the atmospheric response to this warming of the equatorial Pacific (Yualeva et al. 1994). The pressure-weighted mean tropospheric temperature from RSM20th and RSM21st and their differences are shown in Fig. 10a, b, and c, respectively. These temperatures (in Fig. 10) are calculated by taking a pressure-weighted mean of temperatures from 850 to 200 hPa. Figure 10c confirms that tropospheric temperatures in the entire SEUS domain warm in the late twenty-first century relative to the corresponding twentieth-century climatology from the RSM integration. This relative warming of the troposphere results in a stabilization of the atmosphere that is again not conducive to atmospheric convection. To further support this argument of suppression of convection in the SEUS from these large-scale stabilization mechanisms, we show the climatological summer mean surface lifted index (defined in "Appendix") from RSM20th and RSM21st and their differences in Fig. 11a, b, and c, respectively. The difference in the surface lifted index (Fig. 11c) between the two centuries is positive, suggesting the relative inhibition of convection in the late twenty-first century.

As for the differences in the projected summer precipitation between CCSM3-21st and RSM21st, we believe that the significant modulation of the diurnal variability in the latter results in uniform drying across the SEUS. Dai (2006) claimed that CCSM3 showed no improvement over

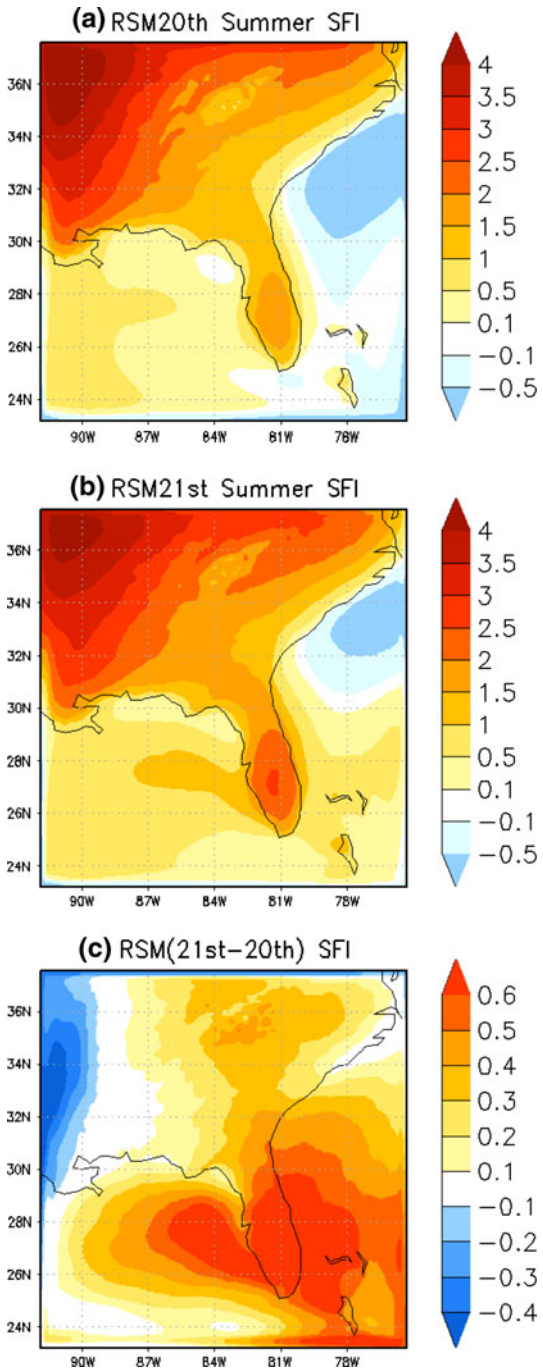

Fig. 11 Same as Fig. 10, but for surface lifted index. Units are in Kelvins

CCSM2 and its erroneous depiction of diurnal variation in most of the globe, including the SEUS. Relative to the ~150-km grid resolution of CCSM3, the grid resolution of 10 km in the RSM simulation is able to resolve the local orographic features, the vegetation distribution, and the coastlines far more reasonably, helping to improve the fidelity of the local diurnal variations (Stefanova et al. 2012). However, the contribution of the model physics at this resolution in the RSM may be equally important for the displayed fidelity of the RSM in terms of its diurnal variations over the SEUS. Poor rendition of the diurnal variation in rainfall negatively impacts the CCSM3 projection of late twenty-first-century summer precipitation over the SEUS. CCSM3 mean summer precipitation under the A2 scenario responds to large-scale forcing and modulation of the NASH and tropospheric stabilization by warmed equatorial Pacific SST. RSM simulations of diurnal variations in SEUS, on the other hand, respond to these large-scale changes, resulting in uniform reduction in rainfall at diurnal peak, which consequently reflects in the mean summer rainfall drying in the late twenty-first century relative to the corresponding mean summer rainfall of the late twentieth century.

Conclusions

We have focused our study of regional climate change on a single variable, precipitation, which we believe is an integrated quantity that reflects important aspects of the total atmospheric response. We discuss the results of regional climate change over the SEUS from one global model (CCSM3 at ~150-km grid resolution) and its dynamically downscaled climate at 10-km grid resolution using the RSM. This study emphasizes on the understanding of the physical mechanisms that produce the model projections more than the absolute magnitude of anticipated changes.

The results of our study, consistent with the results of earlier studies on the subject, show that CCSM3 displays a dipole-like change in the mean summer precipitation for the A2 emission scenario: Peninsular Florida and adjacent oceans dry, and the remainder of the SEUS becomes wetter relative to the corresponding mean summer rainfall of the late-twentieth-century simulation. In the dynamically downscaled simulation using the RSM, the summer precipitation response is different in that it shows a uniform drying across the SEUS. We trace the differences between these model projections to the RSM displaying a reasonable fidelity in depicting the diurnal variations in the summer climate in SEUS. This is in contrast to CCSM3, which displays a poor fidelity of diurnal variations. The RSM indicates a significant reduction in the rainfall during the time of diurnal peak in the late twenty-first century. This reduction in the diurnal maximum rainfall in RSM is in response to large-scale changes in the westward shift of the NASH and the relative warming of the tropospheric temperature resulting from warm SST anomalies in the equatorial Pacific Ocean.

The results we present are of concern to the agriculture industry of the SEUS. In the SEUS agriculture is primarily rain fed (Misra et al. 2011a, b), making it particularly sensitive to rainfall variability. Observations indicate that because of the summer season rainfall, the SEUS is climatologically the wettest region in the conterminous United States (Chan and Misra 2010). Sustaining the multibillion-dollar agriculture industry (Hansen et al. 1998), forecasted to grow in the coming years, imparts an urgency to understanding rainfall changes arising from climate change, especially during the summer growing season over the SEUS. The booming population of the region (Seager et al. 2009) and the ability to meet growing demands for freshwater while simultaneously preventing saltwater intrusion into the aquifers (Karl et al. 2009) are also major concerns in managing water resources. Further studies such as this one are required in order to create a robust collection of outcomes for decision-makers.

Acknowledgments We acknowledge the editorial assistance of Kathy Fearon of COAPS, FSU. This study was supported by grants from NOAA (NA07OAR4310221), USDA (027865), and USGS (06HQGR0125).

Appendix

The surface lifted index (SFI) is a measure of atmospheric stability. It is defined as the difference between the environmental air temperature at 500 mb and the temperature a parcel of air will achieve if lifted dry adiabatically to its lifting condensation level (LCL) and then lifted moist adiabatically to 500 mb. Positive values of SFI are considered to be stable, and negative values are considered unstable.

References

Atkins N, Wakimoto R, Weckwerth T (1995) Observations of the seabreeze front during CaPE. Part II: dual-doppler and aircraft analysis. Mon Wea Rev 123:944–969

Bastola S, Misra V (2013) Sensitivity of hydrological simulations of southeastern United States watersheds to temporal aggregations of rainfalls. J Hydrometeor. doi:10.1175/JHM-D-12-096.1

Biggs W, Graves M (1962) A lake breeze index. J Appl Meteor Climatol 1:474–480

Bove M, Elsner J, Landsea C, Niu X, O'Brien J (1998) Effect of El Niño on U.S. landfalling hurricanes, revisited. Bull Am Soc 79:2477–2482

Briegleb B, Bitz C, Hunke E, Lipscomb W, Holland M, Schramm J, Moritz R (2004) Scientific description of the sea ice component in the community climate system model, version three. Tech. Rep. NCAR/TN-463 + STR, 78 pp

Bukovsky M, Karoly D (2008) An evaluation of climate model precipitation over the United States, 20th conference on climate variability and change, New Orleans, LA. American Meteorological Society, P3.8

Carbone R, Tuttle J (2008) Rainfall occurrence in the U.S. warm season: the diurnal cycle. J Climate 21:4132–4146

Chan S, Misra V (2010) A diagnosis of the 1979–2005 extreme rainfall events in the Southeastern United States with isentropic moisture tracing. Mon Wea Rev 138:1172–1185

Chiang J, Sobel A (2002) Tropical tropospheric temperature variations caused by ENSO and their influences on the remote tropical climate. J Climate 15:2616–2631

Chou MD, Lee KT (1996) Parameterizations for the absorption of solar radiation by water vapor and ozone. J Atmos Sci 53:1203–1208

Chou MD, Suarez MJ (1994) An efficient thermal infrared radiation parameterization for use in general circulation models. Technical report series on global modeling and data assimilation, NASA/TM-1994-104606, 3, 85 pp

Christensen J et al (2007) Regional climate projections. Climate change 2007: the physical science basis. Cambridge University Press, Cambridge

Collins W et al (2004) Description of the NCAR community atmosphere model (CAM3). Tech. Rep. NCAR/TN-464 + STR, 226 pp

Collins W et al (2006) The community climate system model version 3 (CCSM3). J Climate 19:2122–2143

Dai A (2006) Precipitation characteristics in eighteen coupled climate models. J Climate 19:4606–4630

Dickinson R, Oleson K, Bonan G, Hoffman F, Thornton P, Vertenstein M, Yang ZL, Zeng X (2006) The community land model and its climate statistics as a component of the community climate system model. J Climate 19:2302–2324

Doblas-Reyes F, Goodess C (2005) Working paper on the need for downscaling of seasonal-to-decadal integrations within the EU-funded ENSEMBLES project. ENSEMBLES Technical Report No. 2, 10 pp. [ISSN 1752-2854]

Ek M, Mitchell K, Lin Y, Rogers E, Grunmann P, Koren V, Gayno G, Tarpley J (2003) Implementation of Noah Land surface model advances in the national centers for environmental prediction operational Mesoscale Eta Model. J Geophys Res 108:8851

Elguindi N, Grundstein A (2013) An integrated approach to assessing 21st century climate change over the contiguous US using the NARCCAP RCM output. Climatic Change 117:809–827

Hansen J, Hodges A, Jones J (1998) ENSO influences on agriculture in the southeastern United States. J Climate 11:404–411

Hong S, Pan H (1996) Nonlocal boundary layer vertical diffusion in a medium range forecast model. Mon Wea Rev 124:2322–2339

Juang HM, Kanamitsu M (1994) The NMC nested regional spectral model. Mon Wea Rev 122:3–26

Kanamaru H, Kanamitsu M (2007a) Scale-selective bias correction in a downscaling of global analysis using a regional model. Mon Wea Rev 135:334–350

Kanamaru H, Kanamitsu M (2007b) Fifty-seven-year reanalysis downscaling at 10 km (CaRD10). Part II: comparison with North American Regional Reanalysis. J Climate 20:5572–5592

Kanamitsu M, Kanamaru H (2007) Fifty-seven-year reanalysis downscaling at 10 km (CaRD10). Part I: system detail and validation with observations. J Climate 20:5553–5571

Kanamitsu M, Yoshimura K, Yhang Y (2010) Errors of interannual variability and trend in dynamical downscaling of reanalysis. J Geophys Res 115:1–17

Karl T, Melillo J, Peterson T (2009) Global climate change impacts in the United States. Cambridge University Press, Cambridge

Kushnir Y, Seager R, Ting M, Naik N, Nakamura J (2010) Mechanisms of tropical Atlantic SST influence on North American precipitation variability. J Climate 23:5610–5628

LeMone M (1973) The structure and dynamics of horizontal roll vortices in the planetary boundary layer. J Atmos Sci 30:1077–1091

Li W, Li L, Fu R, Deng L, Wang H (2011) Changes to the north Atlantic subtropical high and its role in the intensification of summer rainfall variability in the southeastern United States. J Climate 24:1499–1506

Lin Y, Mitchell K (2005) The NCEP Stage II/IV hourly precipitation analyses: development and applications. Preprints, 19th conference on hydrology, american meteorological society, San Diego, CA, 9–13 January 2005, Paper 1.2

Loveland T, Merchant J, Reed B, Brown J, Ohlen D, Olson P, Hutchinson J (1995) Seasonal land cover regions of the United States. Ann Assoc Am Geogr 85:339–355

Mearns L, Gutowski W, Jones R, Leung L, McGinnis S, Nunes A, Qian Y (2009) A regional climate change assessment program for North America. EOS 90:311–312

Misra V, DiNapoli S (2012) Understanding the wet season variations over Florida. Clim Dyn (in press). doi:10.1007/s00382-012-1382-4

Misra V, Moeller L, Stefanova L, Chan S, O'Brien JJ, SmithIII TJ, Plant N (2011) The influence of the Atlantic warm pool on the panhandle Florida Sea breeze. J Geophys Res. doi:10.1029/2010JD01

Misra V et al (2011b) Climate scenarios: a Florida-Centric view, Florida climate change task force

Neelin J, Chou C, Su H (2003) Tropical drought regions in global warming and El Nino teleconnections. Geophys Res Lett. doi:10.129/2003GLO018625

Oleson K et al (2004) Technical description of the community land model (CLM). Tech. Rep. NCAR/TN-461 + STR, 174 pp

Pan H, Wu W (1995) Implementing a mass-flux convective parameterization package for the NMC medium range forecast model, paper presented at 10th conference on Numerical Weather Prediction. American Meteorological Society, Portland, Oregon

Parker M, Ahijevych D (2007) Convective episodes in the east-central United States. Mon Wea Rev 135:3707–3727

Rauscher S, Kucharski A, Enfield D (2011) The role of regional SST warming variations in the drying of Meso-America in future climate projections. J Climate 24:2003–2016

Schwartz B, Bosart L (1979) The diurnal variability of florida rainfall. Mon Wea Rev 107:1535–1545

Seager R, Tzanova A, Nakamura J (2009) Drought in the southeastern United States: causes, variability over the last millennium, and the potential for future hydro climate change. J Climate 22:5021–5045

Slingo J (1987) The development and verification of a cloud prediction scheme for the ECMWF model. Q J R Meteorol Soc 113:899–927

Smith R, Gent P (2002) Reference manual for the parallel ocean program (POP), ocean component of the Community Climate System Model (CCSM 2.0 and 3.0) Tech. Rep. LA-UR-02-2484, Los Alamos National Laboratory

Sobolowski S, Pavelski T (2011) Evaluation of present and future North American regional climate change assessment program (NARCCAP) regional climate simulations over the southeast United States. J Geophys Res 117. doi:10.1029/2011JD016430

Stefanova L, Misra V, Chan S, Griffin M, O'Brien J, Smith T III (2012) A proxy for high-resolution regional reanalysis for the Southeast United States. Climate Dyn 38:2449–2466

Vecchi G, Clement A, Soden B (2008) Examining the tropical Pacific's response to global warming. Trans Amer Geophys Union 89:81–83

Xie S, Deser C, Vecchi G, Ma J, Teng H, Wittenberg A (2010) Global warming pattern formation: sea surface temperature and rainfall. J Climate 23:966–986

Yualeva E, Holton J, Wallace J (1994) On the cause of annual cycle in the tropical lower stratospheric temperature. J Atmos Sci 51:169–174

Zhang DL, Zhang S, Weaver S (2006) Low-level jets over Mid-Atlantic states: warm-season climatology and a case study. J Appl Meteor Climatol 45:194–209

Zhang X, Dimarco S, Smith D, Howard M, Jochens A, Hetland R (2009) Near-resonant ocean response to sea breeze on a stratified continental shelf. J Phys Oceanogr 39:2134–2155